Front. Phys. China, 2009, 4(3): 327–336
DOI 10.1007/s11467-009-0030-x

REVIEW ARTICLE

The first-principles calculation of molecular conduction

Hao CHEN (陈灏)(✉)

Physics Department, Fudan University, Shanghai 200433, China
E-mail: haochen@fudan.edu.cn

Received January 25, 2009; accepted February 23, 2009

We used the self-consistent method-based density functional theory (DFT) and non-equilibrium Green's function (NEGF) to simulate molecular transport. Our numerical calculations for the organic molecular measurement made by Reichert *et al.* (Phys. Rev. Lett., 2002, 88: 176804) and for the alkanedithiols measurement made by Xu *et al.* (Science, 2003, 301: 1221) met the related experimental values quite well. This means that the first-principles calculations based on DFT and NEGF can well explain the conduction measurements of some large molecules. The numerical study reveals the fact that molecular conduction does not obey the classic law; in stead it illustrates the quantum behavior. We designed active molecular transistors controlled by the gate bias with high working frequency. They may be the next generation electronic devices.

Keywords molecular conduction, molecular transistor, first-principles calculation

PACS numbers 73.23.-b, 85.65.+h, 31.15.Ar

Contents

1 Introduction

Significant advances have been made in silicon-based CMOS devices in the past half century. It is expected that the minimization of semiconductor devices will approach the quantum and economic limit within 10 to 15 years. The search for prospective candidates for silicon-based semiconductor devices has become a worldwide effort. The suggestion that organic molecules may be the next generation devices was initially put forward by Aviram and Ratner in the 1970s [1]. In the recent decade the experimental and theoretical achievements in molecular conduction were made due to the developments of nano-technology, such as scanning tunneling microscopy (STM), atomic force microscopy, self-assembled monolayer methods, mechanically controllable break junction (MCBJ), etc. The current–voltage I–V characteristics of molecular devices show profound potential for applications, including the negative differential resistance and switches, etc. Several experimental groups have reported measurements of the I–V characteristics of some organic small molecules [2−10]. These developments have attracted great interest in modelling and understanding the capabilities of the molecular conductor from the basic scientific and applied point of view [11−23].

Microminiaturization of electronic devices to the molecular scale brings a new complication to the transport study compared with macroscopic systems: the treatment of the contacts between the microscale molecule with the discrete energy levels and the macroscopic electrode with the continuous band structure. For devices of molecular dimension, the contact becomes an important part of the device, and the measured electronic characteristics depend on the coupling in detail. The treatment of molecular devices requires the inclusion of the semi-infinite gold contacts under bias, which combines the theory of quantum transport with the electronic structure theory from the first-principles calculations. And the organic molecule and the macroscopic electrodes should be treated on an equal footing, with the whole open system, lead-molecule-lead, calculated self-

consistently. The first effort for the first-principles calculation of the molecular conduction was made by using the Lippman–Schwinger equation and the jellium model for the semi-infinity leads [12]. The plane wave representation in their calculation was very large to treat the local interface coupling, which prevented the method in the use of the large molecules.

Taylor *et al.* [13] adopted the density functional theory (DFT) associated with the non-equilibrium Green's function (NEGF) method to deal with transport problem of the nanotube system. The method successfully describes the transport behavior of the open system at the level of the electronic structure calculation, and soon was used in the study of the molecular circuit. In Taylor's work, the DFT calculation of the electronic structure was made with the quantum chemistry software Siesta, while Damle [14, 15] and Xue [16] applied the commercial quantum chemistry software Gaussian 98 to do the same work. Both Taylor and Xue used tight-binding parameters obtained by fitting accurate augmented-plane-wave calculation of band-structure to describe contacts of quasi-1-D leads. Damle obtained the data from the DFT calculation of the finite gold cluster first, then calculated the surface Green's function (SGF) of 3-D lattice by the tight-binding method. Following Damle *et al.* [14, 15] we adopted 3-D lattice, based on the DFT tight-binding model, to deal with electrodes [24]. We used the standard quantum chemistry software Gaussian 03 [25], of which the convergency is improved to a large extent, to calculate the electronic structure for both the organic molecule and the macroscopic electrodes and cooperated with the NEGF theory to build the electronic transport theory of the open system. Originally, both Siesta and Gaussian softwares were designed only for the self-consistent calculations of the isolated system, used in quantum chemistry. Now the self-consistent calculations should be extended to the open system in the molecular circuit [12−16, 24].

2 Theory of quantum transport in the first-principles calculations

In the computation of molecular conduction, the sulfur atom is usually used to connect the organic molecule and the gold lead, sitting on the hollow position of its three nearest-neighboring surface gold atoms. The separation between the gold surface and the sulfur atom is about 2.0 Å. The metal/molecule/metal system is partitioned into two parts: the molecule bridging the junction of the gold electrodes, and the lead part, two semi-infinite Au leads (source and drain). The external applied bias drives the system out of equilibrium, and the current through this system is measured at different bias. The calculation is made self-consistently by using DFT cooperated with NEGF formalism.

The retarded Green's function of the molecule is defined as:

$$G_M^R = (E^+ S_M - F_M - \Sigma_1^R - \Sigma_2^R)^{-1} \tag{1}$$

where G_M^R, S_M, F_M are the retarded Green's function, overlap matrix, and Fock matrix of the molecule part, respectively. E^+ denotes energy plus an infinitesimal imaginary part (usually 10^{-5} or 10^{-6}). The retarded self-energy Σ_1^R (Σ_2^R) of the left (right) side, describing the contribution from the semi-infinite lead, is calculated from SGF g_1^R (g_2^R)

$$\sum\nolimits_i^R = (E^+ S_{Mi} - F_{Mi}) g_i^R (E^+ S_{iM} - F_{iM}) \tag{2}$$

with $i = 1, 2$. The coupling matrices S_{Mi} and $F_{M,i}$ are extracted from the DFT calculation for the extended molecule, which includes three sulfur-nearest-neighbor gold atoms on each side. As an improvement, one may include several gold atoms in the molecule, and move the molecule-lead interface inside the gold electrode in the cost of the more computational times.

In the calculation, the lead is treated as a three-dimensional one with the semi-infinite periodic bulk lattice. The SGF in the transversal $\boldsymbol{k}$ space representation is calculated iteratively by the tight binding method in the gold FCC (111) direction:

$$\begin{aligned}(g_{\boldsymbol{k}}^R)^{-1} = {} & E^+ S_{00} - F_{00} - (E^+ S_{01} - F_{01}) \\ & \cdot g_{\boldsymbol{k}}^R (E^+ S_{01}^\dagger - F_{01}^\dagger)\end{aligned} \tag{3}$$

where S_{00}, F_{00} represent the overlap and Fock matrix of the surface layer in $\boldsymbol{k}$ space representation, and S_{01}, F_{01} represent the counterparts between the surface layer and the nearest layer. They are all calculated by the DFT method through Gaussian 03. The SGF in the real space is obtained from the Fourier expansion:

$$g_{s,ij}^R = g_s^R(\boldsymbol{r}_i - \boldsymbol{r}_j) = \frac{1}{N} \sum_{\boldsymbol{k}} g_{\boldsymbol{k}}^R \mathrm{e}^{\mathrm{i}\boldsymbol{k}\cdot(\boldsymbol{r}_i - \boldsymbol{r}_j)} \tag{4}$$

where N is the number of points in the 2-D Brillouin zone, or the number of unit cells in the lead surface (usually, 11×11 unit cell is enough).

The density matrix of the open system is the essential function of the whole self-consistent scheme. It can be achieved by the integration of the Keldysh non-equilibrium Green's function $G^<(E)$

$$\rho = \int_{-\infty}^{\infty} \mathrm{d}E[-\mathrm{i}G^<(E)/(2\pi)] \tag{5}$$

$$-\mathrm{i}G^< = G_M^R (f_1 \Gamma_1 + f_2 \Gamma_2) G_M^A \tag{6}$$

with the advanced Green's function $G^A = (G^R)^\dagger$. The Fermi distribution of the left (right) lead in equilibrium $f_i(E) = 1/(\mathrm{e}^{\frac{E-\mu_i}{kT}} + 1)$, with the chemical potential

$\mu_1 = E_f - \frac{1}{2}eV$ and $\mu_2 = E_f + \frac{1}{2}eV$. The Fermi level E_f of the bulk Au is set as a "common fitting parameter" around the value of the work function (5.31 eV) of the gold FCC structure in (111) direction to explain the experimental results. In our work, E_f is -5.1 eV [15, 16, 24]. The zero point of the electrical potential is set at the symmetrical center of the lead-molecule-lead system. The broadening function of the left (right) lead Γ_1 (Γ_2), which denotes the finite lifetime of electrons, is a real symmetry matrix:

$$\Gamma_{1(2)} = \mathrm{i}\left[\sum\nolimits_{1(2)}^{R} - \sum\nolimits_{1(2)}^{A}\right] \tag{7}$$

In the calculation, the density matrix is partitioned into two parts:

$$\rho = \rho^{\mathrm{eq}} + \rho^{\mathrm{neq}} \tag{8}$$

where the equilibrium state contribution is obtained from the integration along the real axis from $-\infty$ to $E_{\min}$ (below the bottom energy of the molecule valence band) and the one along the semicircle from $E_{\min}$ to E' in the complex contour, respectively (at zero temperature for simplicity)

$$\rho^{\mathrm{eq}} = -I_m\left(\int_{-\infty}^{E_{\min}} + \oint_{E_{\min}}^{E'}\right)\mathrm{d}E G_M^R(E)/\pi \tag{9}$$

$$\rho^{\mathrm{neq}} = \int_{E'}^{\infty}\mathrm{d}E G_M^R(f_1\Gamma_1 + f_2\Gamma_2)G_M^A/(2\pi) \tag{10}$$

It is noted that the second part of Eq. (9) is the contribution from the valence electrons and its first part is from the deep core level electrons, which can be integrated by using $-\mathrm{i}\eta$ to replace the self-energy. To check the accuracy of the density matrix, the electron number of the molecule is the touchstone

$$N = \mathrm{Tr}(\rho S_M) \tag{11}$$

The molecule connected to the contacts under bias has to keep neither the integer number of electrons, nor the neutral states. There are some charges transferred between the molecule and the metal electrodes. The absolute value of the transferred charges $|\delta n|$ for most metal-molecule combinations is usually much less than 1, and the charges transferred are accumulated on the contact surface. Getting the density matrix accurately, we can calculate the total current for coherent transport

$$\begin{aligned} I &= \frac{2e}{h}\int_{-\infty}^{\infty}\mathrm{d}E T(E)[f_2(E) - f_1(E)] \\ &= \frac{2e}{h}\int_{-\infty}^{\infty}\mathrm{d}E \mathrm{Tr}(\Gamma_1 G^R \Gamma_2 G^A)[f_2(E) - f_1(E)] \end{aligned} \tag{12}$$

where $T(E)$ is the transmission function.

The molecular density of states (DOS) is connected to the imaginary part of the retarded Green's function:

$$\mathrm{DOS} = -\mathrm{Im}\ \mathrm{Tr}(G_M^R S_M)/\pi \tag{13}$$

In the whole calculation, the inner cycle of Gaussian 03 for the isolated molecule is replaced by the cycle for the lead-molecule-lead open system under bias based on NEGF.

3 Molecular current: two-order discrepancies between theory and experiments

The first experiment, which proved the conductivity of the organic molecule benzene, was made by Reed *et al.* in 1997 [2], 23 years after the original idea of molecular rectifier was proposed by Aviran and Ratner in 1974 [1]. The experiment successfully measured the *I–V* characteristic and the differential conductance for the benzene-1,4-dithiolate molecule. Then, electron transport through the phenyl dithiol (PDT) attracted intensive experimental and theoretical interest. The main theoretical approach is made in the level of the first-principles calculation in terms of DFT combined with the NEGF method. A great effort has been made theoretically to simulate the experimental *I–V* curve and conductance gap [12, 14−16, 24], and reproduces the shape of the *I–V* curve. Among many theoretical efforts, we built a program with the NEGF formalism as the subroutines of the Gaussian03 software DFT program to realize the first-principles study of the numerical calculation for the organic molecule. Figure 1 illustrates the calculated results for PDT with different distances between the sulfur atom and Au(111) surface (a) 2.0 Å and (b) 2.1 Å, where the sulfur atom sits on the hollow position of three nearest-neighbor surface gold atoms [24]. All of the theoretical results for *I–V* curves of PDT recover only the shape of the experimental current, not the current magnitude. In fact, the reported experimental values for PDT current are two-order smaller than the theoretical results. The reason for the two-order discrepancy is still an open question. It is not clear where the discrepancy comes from. It is from the theoretical side or the experimental one? Fortunately, there are several large organic molecules where the experimental measurements of molecular conductance were recovered by the DFT–NEGF-based first-principles calculations.

Reichert *et al.* [8] measured electron transport through two types of conjugated molecules, asymmetric and symmetric, consisting of several phenyl rings by using the mechanically controlled break junctions. Due to the fact that their measurements were stable and re-producible, their work attracted much attention and received many citations. To investigate the transport behavior of the above organic molecules theoretically, we optimized the

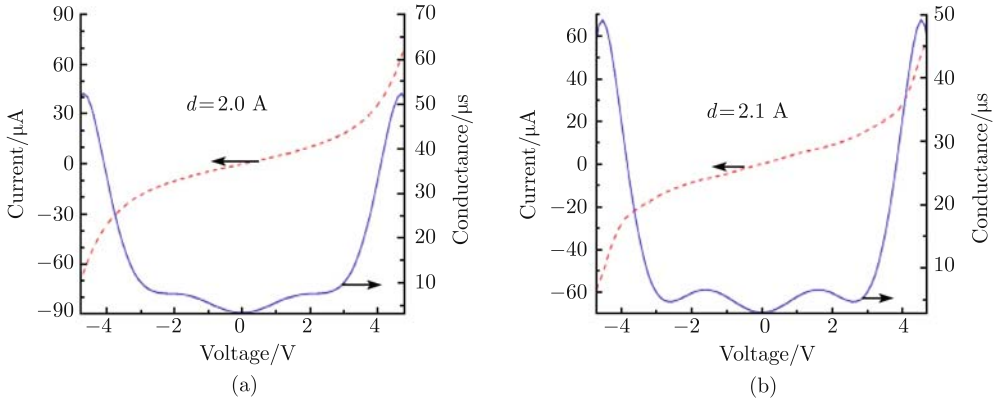

Fig. 1 *I–V* (*dashed*) and differential conductance (*solid*) curves of PDT system. The distance between the sulfur atom and the Au (111) plane is **(a)** 2.0 Å, **(b)** 2.1 Å.

geometrical structures of the two molecules, and obtained the structure consisting of coplanar phenyl rings, with the significant π orbital overlap. Then we calculated the I–V curves at room temperature and low temperature (30 K) through the asymmetric molecule 1,4-Bis ((2'-para-mercaptophenyl)-ethinyl)- 2-acetyl-amino-5-nitro-benzene (called rod 1) and symmetric molecule 9,10-Bis((2'-para-mercaptophenyl)-ethinyl)-anthracene (called rod 2).

The current through the Au-rod 1-Au junction and its numerical differential conductance $\mathrm{d}I/\mathrm{d}V$ at room temperature are given in Fig. 2 [26]. A small plateau around 0.5 V is found at 30 K as indicated by the arrow in Fig. 2. The I–V characteristics are asymmetrical because of the geometrical asymmetry. The calculated current agrees with the measurement very well, especially for bias around ±1.0 V [8, 27]. The corresponding DOS and transmission spectrum are shown in Fig. 3. The system is

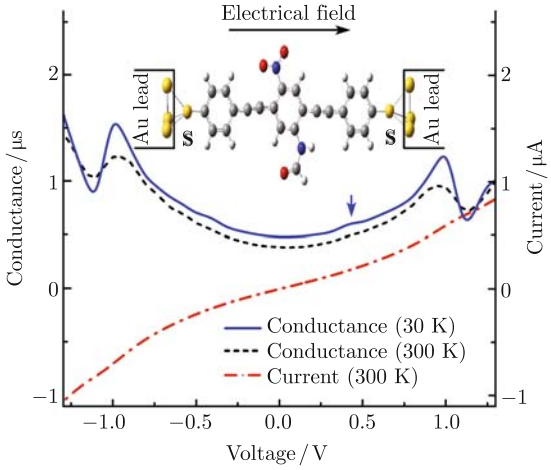

Fig. 2 The current (*dashed–dotted curve*) through the Au-rod 1-Au and its corresponding numerical differential conductance at 30 K (*solid curve*) and 300 K (*dashed curve*). The inset shows the molecule connecting to the Au leads. The direction of the electric field is given in the figure and the down-arrow indicates the small plateau in conductance. For visibility, the conductance at 30 K is offset by +0.1 μs.

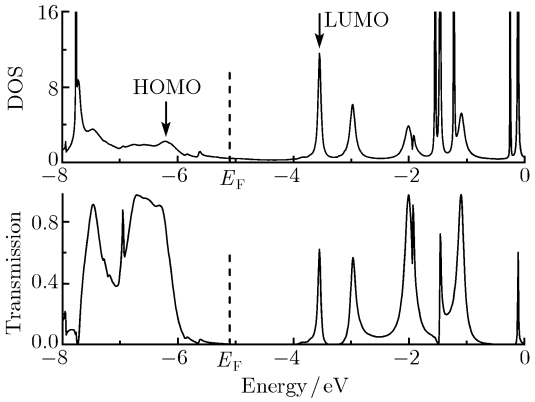

Fig. 3 The DOS and transmission spectrum of rod 1 without bias and at RT (300 K). The dashed lines indicate the position of fermi level. The arrows stand for the HOMO and LUMO of the junction.

called the HOMO-based junction, because the fermi level is close to HOMO level. Although the fermi level lies in the gap between HOMO and LUMO, its DOS near the fermi level is nonzero. The nonzero density of states, stemming from the tail of occupied states and the hybridization of the molecular orbital with the energy band states of Au leads, provides the electrons and holes driven by the external bias. The self-interaction correction (SIC) in DFT calculation with the continuous exchange-correlation approximation opens conduction-gaps in I–V characteristics, which is consistent with the experiments for organic molecular conduction [28].

We also calculated the current through rod 2 and depict the results in Fig. 4. Since the current is very sensitive to the contact of the molecule-electrodes junctions, the different binding site for a molecule between the electrodes, its orientation, and the atomic scale geometry of the molecule-electrode coupling can influence the measurement significantly. Figure 4 gives an example, in which we calculate the current with different couplings to the gold leads. The coupling is determined by the sulfur atom and gold surface separation directly. The solid curve shows the case where the separation between

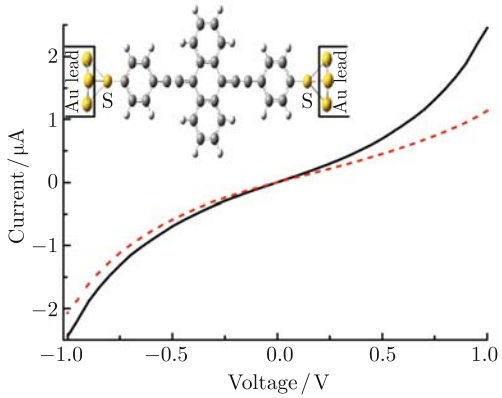

Fig. 4 The current through the Au-rod 2-Au, with the sulfur atoms at the para position. The solid curve represents the case where molecule is coupled to the two leads equally and the dashed curve stands for the current where its couplings are different.

the sulfur atom and its neighboring electrode surface is 2.0 Å. The calculation presents a symmetrical curve due to the identical couplings. If we fix the gold electrodes and shift the molecule to the left electrode by 0.12 Å, an asymmetrical curve (*dashed*) is presented. The asymmetrical measurement occurs frequently in the experiments because of the difficulty in control of the contact between the molecule and the electrode. In order to reveal the distinctive feature, the conductance histogram or statistical analysis is widely used [30, 31]. The topological effect of rod 2 is further studied, as reported by Mayor *et al.* [32] Its geometrical structure, called rod 3, is presented in the inset of Fig. 5. The sulfur atoms connect electrodes through the meta positions and the separation between S atom and gold surface is 2.0 Å. The connection of the meta position changes the electronic structure significantly. Figure 6 illustrates the molecular orbitals of HOMO and LUMO for both isomers, which is important for the transport property. It is found that the HOMO and LUMO of the para position substituted molecule are extensive, which facilitates the current to flow, while for meta substitution, the HOMO and LUMO are localized and the current is insensitive to the bias.

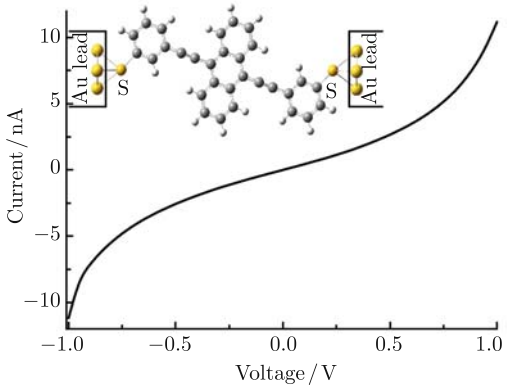

Fig. 5 The topology effect of the Au-rod 3-Au. The inset shows the geometrical structure where the sulfur atoms are in the meta position of the compound.

4 Quantum properties of molecular wires and devices

In molecular electronics the classic theory does not work; electron transport obeys the quantum theory, one of which is the quantum length dependence of conductance of oligothiophene-CH_2 molecules. The calculated I–V characteristics of (n)T1DTs, PPh(n)DTs, and PA(n)DTs are shown in Fig. 7 with multiple thiophene rings (a) or benzene rings (b), (c) [33]. For the oligomer with 2 benzene rings, $n = 2$, PA(2)DT and PPh(2)DT are the same molecule, called naphthalene dithiolate (NaDT) [34]. Before the transport calculations, the optimum structures of (n)T1DTs molecules are achieved from the density functional theory. (n)T1DTs with a small conductance gap have a bigger current than the other two oligomers. Their length dependence of con-

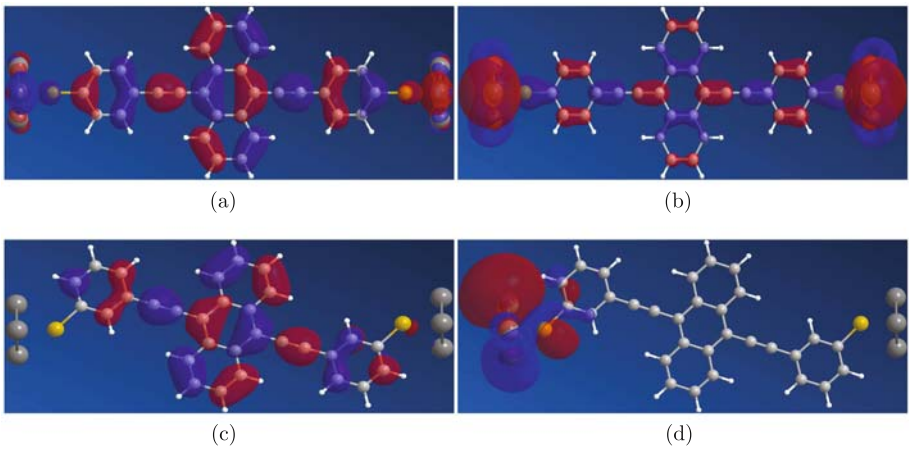

Fig. 6 HOMO (*left*) and LUMO (*right*) orbitals of two isomers with sulphur atoms in the para position (*top panel*) and meta position (*bottom panel*) respectively.

ductance is unusually non-classical under low bias [Fig. 7(a)]: the long oligomers have large conductance, which is well consistent with the experiment results [35], where the authors measured I–V curves for 3T1DT and 4T1DT in the bias regime below 1 V and found that the conductance of 3T1DT is smaller than 4T1DTs'. Not only does our calculated length dependance of conduction for oligomer (n)T1DTs agree with the experiment result, but it also shows a complicated oscillated behavior of the length dependance of conduction for the bias above 1.2 V. Of course, the discrepancy of the absolute magnitude of the current between the calculation and the experiment is quite obvious, about two orders apart. It is also an open question, like the case of benzene current discussed in Section 3.

PPh(n)DTs illustrate the classical-like length dependence under voltage less than 3 V [Fig. 7(b)], and Magoga's exponential law [36] $G = G_{\mathrm{m}}\mathrm{e}^{-\gamma L}$ qualitatively under low bias $V = 0.4$ V [inset of Fig. 7(b)]. Figure 7(c) shows a different conductance length dependence for PA(n)DTs. Under small bias voltage ($V = 0.4$ V), Magoga's conductance exponential law is still satisfied [inset of Fig. 7(c)], which is consistent with the recent experiment results [37]. But at high bias, the exponential law breaks down; some longer molecules have higher conductance than shorter ones, which illustrates an irregu-

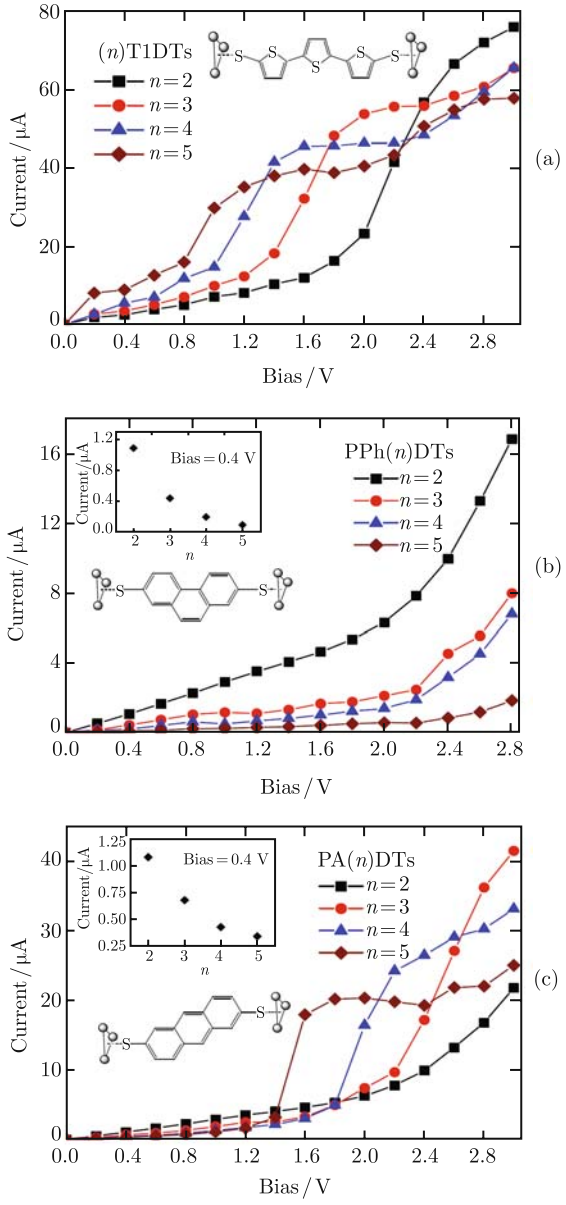

Fig. 7 I–V characteristics of the three oligomers. **(a)** (n)TDTs show the unusual length dependence in the low bias regime, $V < 1.2$ V, and the oscillated length dependence at the high bias. (**b**) PPh(n)DTs show a classical-like length dependence. The inset illustrates the Magoga's exponential law at low bias $V = 0.4$ V. **(c)** PA(n)DTs present the classical-like length dependence at the low bias regime $V < 1.2$ V and the unusual quantum length dependence at the high bias. The inset illustrates the Magoga's exponential law at low bias $V = 0.4$ V.

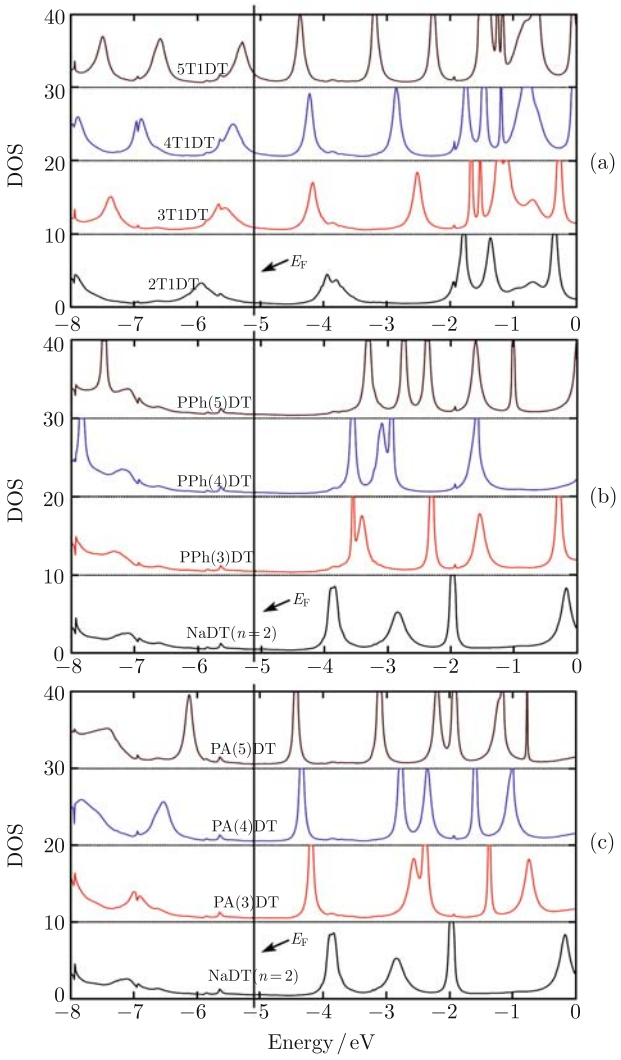

Fig. 8 DOS as a function of energy of the three oligomers with the gold contacts (shifted vertically for visibility). **(a)** For (n)T1DTs, the increase in the number of thiophene ring results in an increase of the value of DOS at E_{F} and a reduction of the HOMO–LUMO gap. **(b)** For PPh(n)DTs, with the increase of benzene ring, DOS at E_{F} decreases and and the HOMO–LUMO gap increases. **(c)** For PA(n)DTs, with the increase of benzene ring, both DOS at E_{F} and the HOMO–LUMO gap decrease.

lar conductance oscillation with respect to the molecular length.

The investigation for non-equilibrium transport of electrons in molecular electronics is based on the molecular orbital theory, while the distribution of the molecular levels determines the transport property. Coupling between the molecule and Au electrodes plays an important role in electronic transport, which expands the discrete molecular levels to a continuous spectrum of density of stats (DOS). Figure 8 illustrates the DOS of equilibrium for the three types of oligomers sandwiched between two gold electrodes, which dominates the molecular transport behavior.

To investigate the exponential law of the alkanedithiols, we calculated their I–V characteristics. The results are plotted in two figures, Fig. 9(a) and (b) [38]. The small applied bias (less than 0.2 V) keeps the exponential law valid, where only tunneling transmission occurs without resonant transmission. In the tunneling regime, the I–V curves will keep linear. At a given bias, the current decreases sharply when the number of methylene in alkane increases, which is just the exponential decay law [39, 40]. The resistance of the lead-molecule-lead system conforms with Magoga's exponential law, $R = R_0 \exp(\gamma L)$. Although the measured values of the conductance damping factor γ are in accordance with each other, the contact resistance R_0 is a bit controversial. The measured values of R_0 in the past years dispersed in a large region. The situation has improved in recent years, with the measured values of the contact resistance R_0 reduced from the early values of 10^7 Ω [41−43] to the recent values of 10^4 Ω [10, 44, 45]. In Fig. 10 our calculated value of the contact resistance R_0 is in good consonance with the result of Ref. [10]. This is another good example of the calculated results conforming with the experiments in molecular electronics.

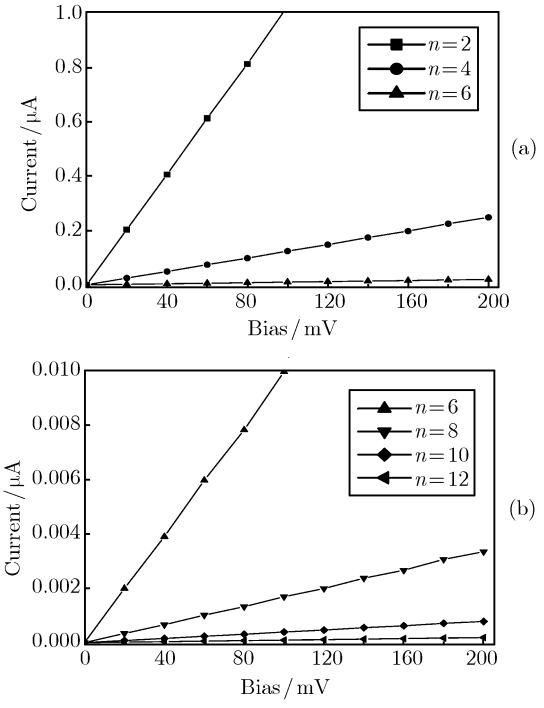

Fig. 9 I–V characteristics of the n-alkanedithiols for **(a)** $n = 2, 4, 6$ and **(b)** for $n = 6, 8, 10, 12$. Putting the results into two plots is for clarity.

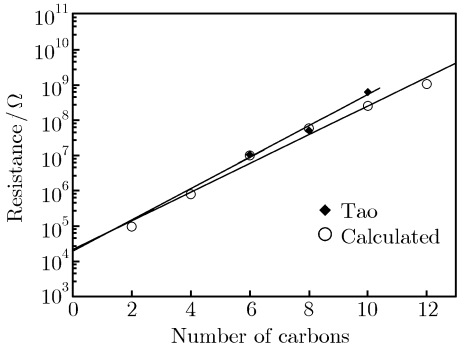

Fig. 10 Semilog of the resistance versus the number of methylenes in alkanedithiols. Our calculated results (*circles*) are in good agreement with the results of Ref. [10] (*diamonds*).

5 Molecular transistors

Finding new active molecular devices has been one of the main goals in the study of molecular electronics. Organic molecules can be used as the electronic switch to control their electronic transport properties by electrical or photo signals.

Reed *et al.* [46] reported a molecular switch consisting of three aromatic phenyl rings in series. The middle ring of the molecule 2′-amino-4-ethynylphenyl-4′-ethynylphenyl-5′-nitro- 1-benzenethiol rotates with respect to the side benzene rings. The dipole composed of donor NH_2 and acceptor NO_2, attached to the middle benzene, is driven by the external field to switch the molecule between on and off states. We calculated its switch behavior and illustrated the effect of the molecular configuration on the switch current [47]. The energy levels of the isolated molecule corresponding to the different rotations are illustrated by the inset of Fig. 11. With leads attached, the self-energy effect and the charge effect cause the molecular energy levels to be broadened and shifted. In Fig. 11 the I–V curves are steep for $\alpha \leqslant 30°$, since both HOMO and LUMO are responsible for the rising of current. From 30° to 60°, the switch effect due to the rotation is more apparent than the case $\alpha \leqslant 30°$.

We designed a bistable molecular switch, triggered between two molecule configurations by using an applied electric field [48]. The switch has two chiral states that share very similar electronic structure originally. The molecular switch is a stator–rotor switch, consisting of the stationary bridge (stator) and the –NH_2 donor group (rotor). The Coulomb interaction between the donor and the two hydrogen atoms at the low part of the stator

causes two stable states for the system. The charging effect, which changes the electronic structures in different way, causes the I–V curves to be distinguishable. Figure 12 presents the configuration of the molecular switch, which has good switch performance with large ratio $I_{\text{state1}}/I_{\text{state0}}$.

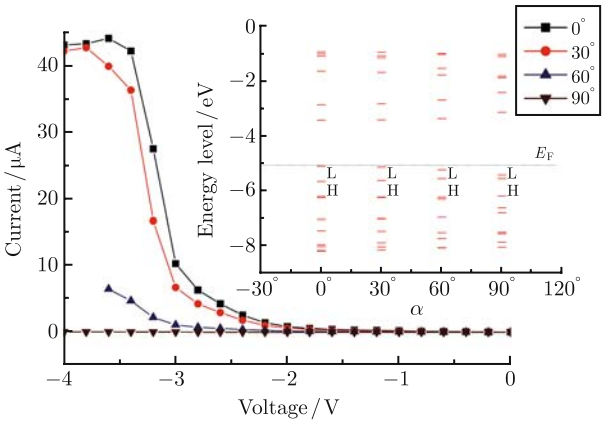

Fig. 11 I–V curves of 2′-amino-4-ethynylphenyl-4′-ethynylphenyl-5′-nitro-1-benzenethiol with gold contacts through sulfur atoms from both sides corresponding to $\alpha = 0°$, $30°$, $60°$, and $90°$. The inset shows the corresponding energy levels of the isolated molecule.

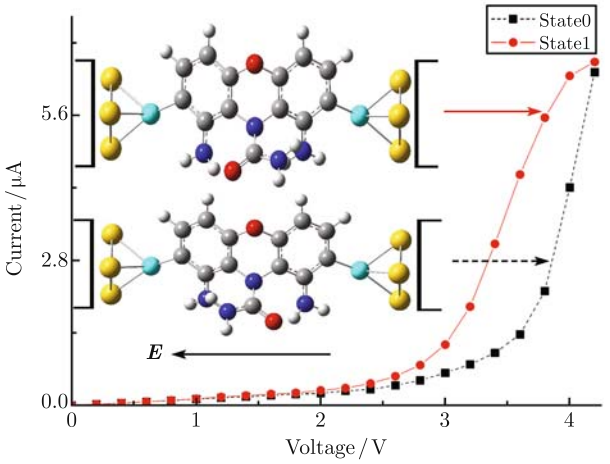

Fig. 12 I–V characteristics for donor –NH2, and their geometries of two states.

The goal of our research was to build the molecular transistor used in the CPU of the computer. The molecular transistors should work at very high frequency. We designed several kinds of molecular devices to meet the requirement [49]. They are all driven by the transverse electric field, and work without any configuration variations. To present the possibility of organic molecular devices controlled by the gate bias, the I–V characteristic of several molecular transistors are illustrated with the electron number deviation from the equilibrium state. Figure 13 shows the I–V curve for three-fused-ring thiophene (a) and seven-fused-ring thiophene (b). The pentacene-dithiol (Fig. 14) and five-number-anthracene-dithiol (Fig. 15) also illustrated the good controllable property with good potential as the next generation electronic devices.

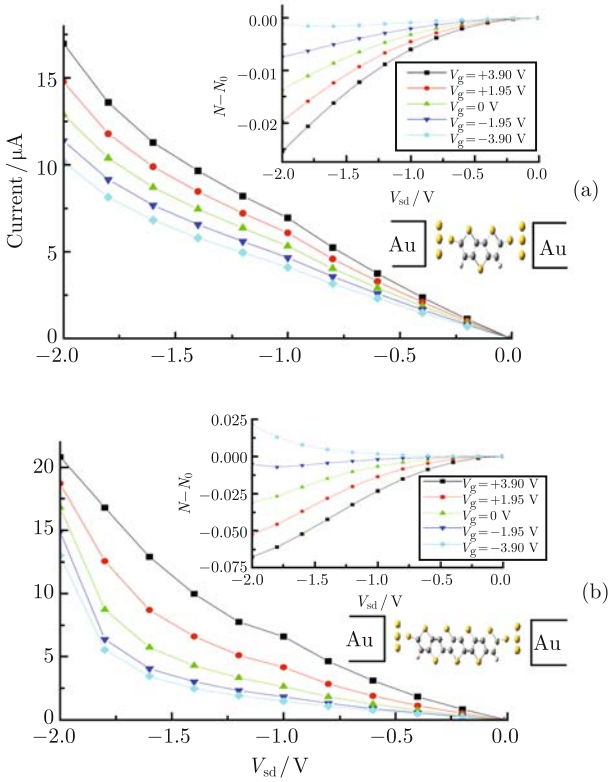

Fig. 13 I–V curves of two fused-ring thiophenes corresponding to the different transverse field: 3-fused-ring thiophene **(a)**, 7-fused-ring thiophene **(b)**. The inset shows the α electron number deviation from the equilibrium state with the modulation of bias.

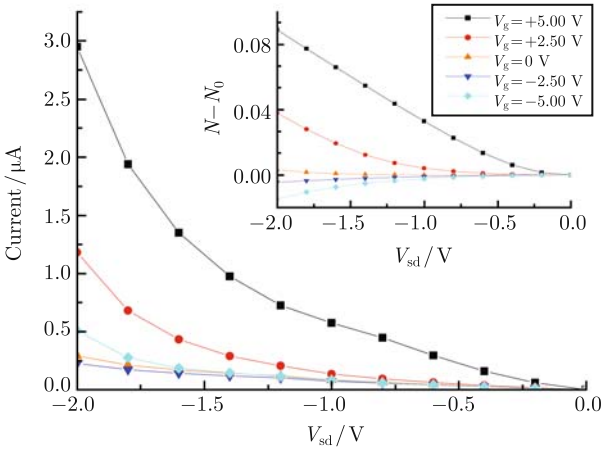

Fig. 14 I–V curves of pentacene-dithiol corresponding to the different gate bias. The inset shows the variation of α electron number relative to that in equilibrium with the change of bias.

The numerical results show that it is possible to control the current through the molecular devices by the gate bias. Organic molecules consisting of the phenyl ring present the strong potential to be molecular transistors with high operation frequency.

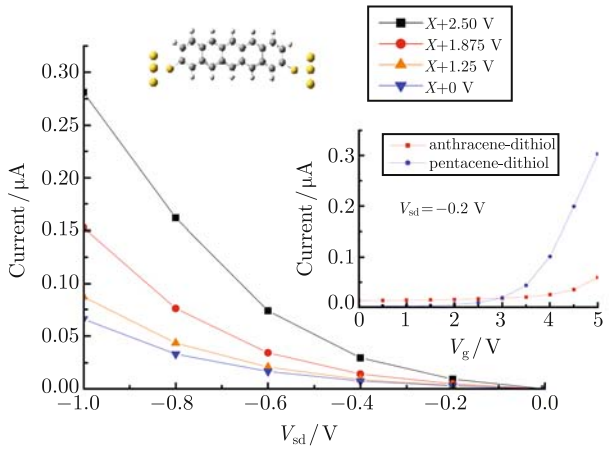

Fig. 15 I–V curves of anthracene-dithiol corresponding to the different gate bias. The inset shows the transfer characteristic curves of anthracene-dithiol and pentacene-dithiol corresponding to the $V_{sd} = -0.2$ V.

6 Summary

We used the self-consistent method based on DFT and NEGF to simulate molecule transport. We expected to solve transport problem from the first-principles calculations in order to predict the transport characteristics of organic molecules and identify the experimental results from the theoretical point of view. We used Gaussian 03 to obtain the electronic structure and at the same time, with breaking the self-consistent iteration cycle inside Gaussian, to replace the density matrix of the isolated molecule with the density matrix of the open system, and run self-consistent iteration until the density matrix converges within an acceptable accuracy.

Although there are still two-order discrepancies of molecular conduction between theory and experiments for the simplest conjugated molecule, the benzene-1,4-dithiol, after 10 years effort [8], we have made some advances to approach the open question in the study of molecular conduction. Our numerical calculations for the organic molecular measurement made by Reichert *et al.* [8] and for the alkanedithiols measurement made by Xu *et al.* [10] meet the related experimental values quite well. It is important evidence: the first-principles calculations based on DFT and NEGF can explain the measurements of some large molecules. For the single benzene, the distance between two electrodes is very small, which makes the conduction measurement very difficult. It is expected that the improved experiments may overcome the two-order discrepancies of benzene conduction between theory and experiments.

The study of the quantum properties of molecular wires and the design of molecular transistors are interesting research areas, which may lead to the birth of the next generation electronic devices. Besides the study of the inelastic current–voltage spectroscopy of single molecule [22, 23], the self-interaction correction in DFT [50], and molecular spintronics [51] have achieved much advances in recent years. We expect the significant progress in the active direction.

Acknowledgements We thank Dr. F. Jiang, Dr. Y. X. Zhou, Dr. Y. Y. Liang, Mr. R. Note, Prof. H. Mizuseki, and Prof. Y. Kawazoe for their contribution. This work was supported by the National Natural Science Foundation of China (Grant Nos. 90606024 and 10574024) and the National Basic Research Program of China (973 Project)(Grant No. 2006CB 921302). We are thankful for the support from Fudan High-end Computing Center, Shanghai Supercomputer Center, and the SR11000 supercomputer from the Center for Computational Materials Science of Institute for Materials Research, Tohoku University.

References

1. A. Aviram and M. A. Ratner, Chem. Phys. Lett., 1974, 29: 277
2. M. A. Reed, C. Zhou, C. J. Muller, T. P. Burgin, and J. M. Tour, Science, 1997, 278: 252
3. J. Chen, M. A. Reed, A. M. Rawlett, and J. M. Tour, Science, 1999, 286: 1550
4. D. I. Gittins, D. Bethell, D. J. Schriffrin, and R. J. Nichols, Nature, 2000, 408: 67
5. X. D. Cui, A. Primak, X. Zarate, J. Tomfohr, O. F. Sankey, A. L. Moore, T. A. Moore, D. Gust, G. Harris, and S. M. Lindsay, Science, 2001, 294: 571
6. J. Park, A. N. Pasupathy, J. I. Goldsmith, C. Chang, Y. Yaish, J. R. Petta, M. Rinkoski, J. P. Sethna, H. D. Abruna, P. L. Mceuen, and D. C. Ralph, Nature, 2002, 417: 722
7. W. Liang, M. P. Shores, M. Bockrath, J. R. Long, and H. Park, Nature, 2002, 417: 725
8. J. Reichert, R. Ochs, D. Beckmann, H. B. Weber, M. Mayor, and H. v. Löhneysen, Phys. Rev. Lett., 2002, 88: 176804
9. R. H. M. Smit, C. Untiedt, G. Rubio-bollinger, R. C. Segers, and J. M. van Ruitenbeek, Phys. Rev. Lett., 2002, 91: 076805
10. B. Xu and N. J. Tao, Science, 2003, 301: 1221
11. W. Tian, S. Datta, S. H. Hong, R. Reifenberger, J. I. Henderson, and C. P. Kubiak, J. Chem. Phys., 1998, 109: 2874
12. M. Di Ventra, S. T. Pantelides, and N. D. Lang, Phys. Rev. Lett., 2000, 84: 979
13. J. Taylor, H. Guo, and J. Wang, Phys. Rev. B, 2001, 63: 245407
14. P. S. Damle, A. W. Ghosh, and S. Datta, Phys. Rev. B, 2001, 64: 201403(R)
15. P. S. Damle, A. W. Ghosh, and S. Datta, Chem. Phys., 2002, 281: 171
16. Y. Xue and M. A. Ratner, Phys. Rev. B, 2003, 68: 115406
17. H. Chen, J. Q. Lu, J. Wu, R. Note, H. Mizuseki, and Y. Kawazoe, Phys. Rev. B, 2003, 67: 113408
18. C. Zhang, M. H. Du, H. P. Cheng, X. G. Zhang, A. E. Roitberg, and J. L. Krause, Phys. Rev. Lett., 2004, 92: 158301
19. F. Evers, F. Weigend, and M. Koentopp, Phys. Rev. B, 2004, 69: 235411

20. P. Delaney and J. C. Greer, Phys. Rev. Lett., 2004, 93: 036805
21. S. H. Ke, H. U. Baranger, and W. Yang, J. Chem. Phys., 2005, 122: 074704
22. M. Galperin, M. A. Ratner, and A. Nitzan, J. Phys.: Condens. Matter, 2007, 19: 103201
23. M. Paulsson, T. Frederiksen, H. Ueba, N. Lorente, and M. Brandbyge, Phys. Rev. Lett., 2008, 100: 226604
24. F. Jiang, Y. X. Zhou, H. Chen, R. Note, H. Mizuseki, and Y. Kawazoe, Phys. Rev. B, 2005, 72: 155408
25. M. J. Frisch, G. W. Trucks, H. Schlegel, et al., Gaussian 03, Revision D. 01, Gaussian, Inc., Wallingford CT, 2004
26. Y. Y. Liang, Y. X. Zhou, H. Chen, R. Note, H. Mizuseki, and Y. Kawazoe, J. Chem. Phys., 2008, 129: 024901
27. J. Reichert, H. B. Weber, M. Mayor, and H. V. Löhneysen, Appl. Phys. Lett., 2003, 82: 4137
28. C. Toher, A. Filippetti, S. Sanvito, and K. Burke, Phys. Rev. Lett., 2005, 95: 146402
29. J. F. Dobson, G. Vignale, and M. P. Das, Electronic Density Functional Theory: Recent Progress and New Directions, New York: Plenum, 1998
30. E. Lörtscher, H. B. Weber, and H. Riel, Phys. Rev. Lett., 2007, 98: 176807
31. F. Chen, J. Hihath, Z. Huang, X. Li, and N. J. Tao, Annu. Rev. Phys. Chem., 2007, 58: 535
32. M. Mayor, H. B. Weber, J. Reichert, M. Elbing, C. von Hänisch, D. Beckmann, and M. Fischer, Angew. Chem. Int. Ed., 2003, 42: 5834
33. Y. X. Zhou, F. Jiang, H. Chen, R. Note, H. Mizuseki, and Y. Kawazoe, Phys. Rev. B, 2007, 75: 245407
34. Z. Crljen, A. Grigoriev, G. Wendin, and K. Stokbro, Phys. Rev. B, 2005, 71: 165316
35. B. Q. Xu, X. L. Li, X. Y. Xiao, H. Sakaguchi, and N. J. Tao, Nano Lett., 2005, 5: 1491
36. E. W. Wong, C. P. Collier, M. Behloradsky, F. M. Raymo, J. F. Stoddart, and J. R. Heath, J. Am. Chem. Soc., 2000, 122: 5831
37. T. Tada, D. Nozaki, M. Kondo, S. Hamayama, and K. Yoshizawa, J. Am. Chem. Soc., 2004, 126: 14182
38. Y. X. Zhou, F. Jiang, H. Chen, R. Note, H. Mizuseki, and Y. Kawazoe, J. Chem. Phys., 2008, 128: 044704
39. M. P. Samanta, W. Tian, S. Datta, J. I. Henderson, and C. P. Kubiak, Phys. Rev. B, 1996, 53: 7626(R)
40. M. Magoda and C. Joachim, Phys. Rev. B, 1997, 56: 4722
41. X. D. Cui, A. Primak, X. Zarate, J. Tomfohr, O. F. Sankey, A. L. Moore, T. A. Moore, D. Gust, G. Harris, and S. M. Lindsay, Science, 2001, 294: 571
42. X. D. Cui, A. Primak, X. Zarate, J. Tomfohr, O. F. Sankey, A. L. Moore, T. A. Moore, D. Gust, L. A. Nagahara, and S. M. Lindsay, J. Phys. Chem. B, 2002, 106: 8609
43. W. Haiss, R. J. Nichois, H. van Zalinge, S. J. Higgins, D. Bethell, and D. J. Schiffrin, Phys. Chem. Chem. Phys., 2002, 6: 4330
44. V. B. Engelkes, J. M. Beebe, and C. D. Frisbie, J. Am. Chem. Soc., 2004, 126: 14287
45. X. Li, J. He, J. Hihath, B. Xu, S. M. Lindsay, and N. Tao, J. Am. Chem. Soc., 2006, 128: 2135
46. M. A. Reed and J. M. Tour, Sci. Am., 2000, 282: 86
47. F. Jiang, Y. X. Zhou, H. Chen, R. Note, H. Mizuseki, and Y. Kawazoe, Phys. Lett. A, 2006, 359: 487
48. Y. Y. Liang, F. Jiang, Y. X. Zhou, H. Chen, R. Note, H. Mizuseki, and Y. Kawazoe, J. Chem. Phys., 2007, 127: 084107
49. F. Jiang, Y. X. Zhou, H. Chen, R. Note, H. Mizuseki, and Y. Kawazoe, J. Chem. Phys., 2006, 125: 084710
50. J. P. Perdew and A. Zunger, Phys. Rev. B, 1981, 23: 5048
51. A. R. Rocha, V. M. Garcia-suarez, S. W. Bailey, C. J. Lambert, J. Ferrer, and S. Sanvito, Nature Mater., 2005, 4: 335